Model-based fault detection, fault isolation and fault-tolerant control of a blade pitch system in floating wind turbines

Seongpil Cho[1, 2], Zhen Gao[1, 2] and Torgeir Moan[1, 2]

[1] Department of Marine Technology, Norwegian University of Science and Technology (NTNU), Trondheim, Norway.
[2] Centre for Autonomous Marine Operations and Systems (AMOS), Norwegian University of Science and Technology (NTNU), Trondheim, Norway.

Abstract

This paper presents model-based fault detection, fault isolation, and fault-tolerant control schemes focused on blade pitch systems in floating wind turbines. Fault detection, isolation, and accommodation techniques are required to achieve high power capture efficiency and structural reliability in floating wind turbines. Faults in blade pitch systems should be detected at an early stage to prevent catastrophic failures. To detect faults of the blade pitch systems, a Kalman filter is designed to estimate the blade pitch angle of the system. The fault isolation algorithm is based on inference methods and capable of determining the fault type, location, magnitude and time. The fault-tolerant controller based on a reconfiguration block with a virtual sensor and shutdown mode controls the floating wind turbine to avoid unexpected external loads. The proposed methods are demonstrated in case studies with stochastic wind and wave conditions that considering different types of faults, such as biases and fixed outputs in pitch sensors and stuck pitch actuators. The simulation results show that the proposed methods can detect and isolate multiple faults effectively at an early stage. Additionally, the effectiveness of the fault-tolerant control systems for different load cases for single and multiple fault conditions is verified by numerical simulations.

Keywords

Floating wind turbine, fault detection and isolation, fault-tolerant control, Kalman filter, Virtual sensor

Corresponding author

E-mail: seongpil.cho@ntnu.no

Abbreviations

FDI	fault detection and isolation
FTC	fault-tolerant control
FWT	floating wind turbine
LMI	linear matrix inequality
MF#	number (#) of multiple faults
NC	nominal PI control
NREL	National Renewable Energy Laboratory
NTM	normal turbulence model
NWP	normal wind profile model
PAS	stuck in pitch actuator
PSB	bias value in pitch sensor
PSF	fixed value in pitch sensor
TF	time of fault occurrence
TFD	time of fault detection

TFI time of fault isolation
TFTC time of fault-tolerant control

1. Introduction

The wind energy industry has experienced rapid growth because of environmental issues and the demand for sustainable solutions. Offshore wind technology in particular has experienced rapid development in recent years, with an annual cumulative global installed capacity of 12.105 GW by the end of 2015 [1]. Historically, most wind turbines were installed in shallow water on bottom-fixed substructures. Currently, offshore wind farms are moving further into deeper water at an average distance of 43.3 km [2] from the shore to capture the high wind energy density. In deeper water, floating wind turbines are more cost effective than bottom-fixed wind turbines. Development projects for floating wind turbines are emerging, including the Hywind 2 project in Scotland and the WindFloat Atlantic and Pacific project in the USA.

Floating wind turbines operate in stochastic ocean environments, such as turbulent winds, irregular waves, and significant disturbances, and they might experience unexpected failures that could lead to system interruptions and cause huge economic losses. Therefore, maintenance and optimal operations of floating wind turbines become critical issues because of limited access. The reliability of an offshore wind turbine is even more important because maintenance costs account for 30% of the overall cost of energy [3]. Faults in wind turbines occur in the sensors, actuators, and system components, and faults with the potential to propagate to turbine failures change the system behavior, the operational safety, and the power production efficiency of the wind turbines. Consequently, wind turbine failure rates should be reduced to ensure reliability and decrease downtime.

A nominal controller may be inefficient and unstable under fault conditions. To supervise potential faults in sensors, actuators or other components, different control techniques are needed. These methods are called fault detection and isolation (FDI) and fault-tolerant control (FTC) techniques. The FDI technique can provide the operator with valuable information on the type, location, and magnitude of the fault. The FTC is a dynamic system that can compensate for sensor and actuator faults by interacting with any pre-existing nominal controllers to cancel the fault effects on the system. The FTC consists of reconfiguration blocks that are linked to the nominal controller in fault conditions. The FDI and FTC techniques use real-time sensor data to clearly detect, isolate and accommodate the wind turbine faults to improve their reliability and reduce the cost of repairs.

The FDI and FTC of wind turbines have been subjected to intensive research. FDI techniques are based on model-based methods and signal-processing methods. For the model-based methods, the system model could be mathematical or knowledge-based. Faults are detected based on residual generation by state variables or parameter estimations. Chen et al. [4] and Wei et al. [5] proposed model-based FDI schemes using a diagnostic observer for the pitch system and drive train faults to the benchmark model. A diagnostic technique for imbalance fault identification based on a probabilistic neural network was presented by Malik et al. [6]. For signal-processing-based fault detection, mathematical or statistical operations are performed on the measurements. Fault detection and isolation schemes applying data-driven design methods to avoid difficult modeling were used by Dong et al. [7]. Santos et al. [8] presented a multi-sensory system combined with a data-mining solution for fault diagnosis and classification using support vector machines in wind turbines. Ghane et al. [9] and Feng et al. [10] demonstrated statistical change detection for a gearbox model of a wind turbine using frequency analysis.

Fault-tolerant control methods can be divided into two categories: passive and active FTC methods [11]. In passive FTC systems, the controllers are fixed control systems predetermined to be robust against faults and uncertainties throughout the entire system. Passive FTC methods are optimized while satisfying a specific fault scenario, which implies that it has limited fault-tolerant capabilities for various faults. Additionally, this approach does not need FDI schemes and controller reconfiguration. Active FTC methods react to system component failures by reconfiguring control references so that acceptable performance and stability of the system can be maintained. An active FTC relies on an FDI scheme, which should feed real-time information to accommodate the faults by reconfiguring control references in the system. Shi and Patton [12] proposed an active fault-tolerant control approach based on an extended state observer to an offshore wind turbine model. By using a bank of virtual sensors and actuators, Seron et al. [13] suggested a FTC scheme that manages sensor and actuator faults. Fan et al. [14] proposed an FTC scheme that is a combination of model reference adaptive control with neural network compensation. Vidal et al. [15] presented a disturbance compensator for controllers to estimate actuator faults and design fault-tolerant controllers.

Fault occurrence rates and their effects are an important factor in the design of wind turbines. Carroll et al. [16] showed the results of an analysis determining the failure rates for the repair of modern offshore wind turbines and their sub-assemblies. According to this study, the blade pitch systems have the highest failure rates among the components and account for 13.3% of the total failures of wind turbines. The blade pitch system is critical for pitch-regulated variable-speed wind turbines, and the relevant faults change the aerodynamic load and power output immediately and thus affect the response of the tower and support structures. The main faults of the blade pitch system occur in the blade pitch sensors and actuators. These faults influence the control feedback and result in imbalanced loads on the rotor, shaft, and main bearings. The detection of faults allows for fast accommodation to avoid catastrophic long-term damage to the wind turbines. The effect of pitch system faults on turbine performance and platform motion in wind turbine components has been studied in recent years for specific fault scenarios [17]-[19].

This paper focuses on model-based FDI and FTC methods in the blade pitch sensors and actuators of a floating wind turbine model. Faults generated in blade pitch sensors and actuators can be detected by a Kalman filter based on residual generation and an appropriate evaluation method. The simple cases of faults, such as bias (PSB) and fixed values in pitch sensors (PSF) and stuck in pitch actuators (PAS), are predetermined by the fault magnitude, type and occurrence time to verify the feasibility of the FDI method. The FTC for the fault scenarios considered in this paper provides a complete solution for immediately accommodating faults. The objectives of this work are as follows:

- Present detection and isolation strategies for different types of faults that might occur in the blade pitch system;
- Design an active fault-tolerant controller to achieve satisfactory performance when all control components are back to functioning normally after a fault occurs; and
- Verify the effectiveness of the proposed FDI and FTC schemes under blade pitch system faults by comparing the structural load, response, and safety of floating wind turbines and considering different wind and wave conditions.

This paper is organized as follows. Section 2 describes the floating wind turbine model, baseline controller, blade pitch system and faults. Section 3 introduces the fault detection, fault isolation, and fault-tolerant control schemes for the blade pitch system. Section 4 describes environmental load cases, such as waves and aerodynamic loads, acting on the floating wind turbine. Section 5 presents

the simulation results for the fault detection and isolation technique according to a residual method and fault decision and accommodation according to a fault detection criterion. Section 6 provides the conclusions.

2. Methodology

2.1. Floating wind turbine concept

A floating wind turbine is modeled as a rotor, nacelle, tower, floater, and mooring system. The model in this paper is based on the variable-speed pitch-regulated NREL 5 MW offshore wind turbine model [20] supported by the spar buoy floater (OC3-Hywind) [21] and three catenary mooring lines as shown in Figure 1. The specifications of the NREL 5 MW reference wind turbine are provided in Table 1. Additionally, properties for the OC3-Hywind floater are listed in Table 2.

2.2 Fully coupled numerical model

The dynamic behavior of the floating wind turbine model is simulated with the Simo-Riflex-Aerodyn software (SRA) [22], which is an aero-hydro-servo-elastic code for fully coupled nonlinear time-domain numerical simulations of offshore wind turbines while simultaneously considering the aerodynamics, hydrodynamics, structural dynamics and mooring line dynamics with an control code for a proportional-integral (PI) pitch and a torque controller under various operational conditions. Models coded by JAVA are added to the SRA to account for the pitch actuator and sensor. Fault data in the blade pitch system are provided in the input file of the SRA to test the feasibility of the fault detection.

2.3. Baseline controller

The baseline control system includes two separate controllers for regulating blade pitch angles and generator torque. The operational region is divided into below-rated and above-rated regions of wind speed. Below the rated wind speed within low wind speeds, the control strategy is to capture the maximum power by adjusting the generator torque and maintaining the optimal tip speed of the blades [20]. Within this region, the blade pitch controller is not active and maximum power is achieved by adjusting the generator torque and then the rotation speed.

Above the rated wind speed, the blade pitch system controls the blade pitch angle to keep aerodynamic loads within specified limits by producing a rated power output at a constant rotor speed. A constant-torque variable pitch controller is used for floating wind turbines to improve the dynamic response of the system and reduce the motion of the floater response to stability issues [23] by modifying the gains of the controller [21]. A blade pitch reference is calculated based on the gain-scheduled PI controller as a function of the generator torque error based on a constant-torque strategy [21] for floating wind turbines.

2.4. Blade pitch system

A commonly used blade pitch system consists of three identical independent pitch actuators and sensors with PI controllers. Regulating each blade pitch angle individually, a 2nd-order pitch actuator is modeled for the 5 MW wind turbine. Consider the blade pitch system that describes a blade pitch reference from the PI controller and the pitch angle measurement:

$$\ddot{\beta}_i + 2\zeta\omega_n\dot{\beta}_i + \omega_n^2\beta_i = \omega_n^2\beta_C \text{ , } i = 1, 2 \text{ and } 3 \text{ (the blade number)} \quad (1)$$

where ζ is the damping ratio, ω_n is the natural frequency of the actuator, and $(\dot{})$ represents the time derivatives. The parameters are ω_n = 11.11 rad/s and ζ = 0.6 [24]. Additionally, β_i is the i^{th} blade pitch angle, and β_C is the blade pitch command.

The recorded measurements must be accurate and reliable because the turbine monitoring and control are based on sensor data during wind turbine operations. A discretized control system that includes process and measurement noises are used in this paper. Process and measurement noises in a state-space model of the blade pitch system described by Eq. (2) are zero-mean Gaussian white noises.

$$\begin{aligned} \dot{\mathbf{x}}(t) &= \mathbf{A}\mathbf{x}(t) + \mathbf{B}\mathbf{u}(t) + \mathbf{w}(t) \\ \mathbf{y}(t) &= \mathbf{C}\mathbf{x}(t) + \mathbf{v}(t) \end{aligned} \tag{2a}$$

or

$$\begin{aligned} \dot{\mathbf{x}}(t) &= \begin{bmatrix} \dot{\boldsymbol{\beta}}_i(t) \\ \ddot{\boldsymbol{\beta}}_i(t) \end{bmatrix} = \begin{bmatrix} \mathbf{0}_{3\times3} & \mathbf{I}_{3\times3} \\ -\omega_n^2\,\mathbf{I}_{3\times3} & -2\omega_n\zeta\,\mathbf{I}_{3\times3} \end{bmatrix} \begin{bmatrix} \boldsymbol{\beta}_i(t) \\ \dot{\boldsymbol{\beta}}_i(t) \end{bmatrix} + \begin{bmatrix} \mathbf{0}_{3\times3} \\ \omega_n^2\,\mathbf{I}_{3\times3} \end{bmatrix} \boldsymbol{\beta}_{C,i}(t) + \begin{bmatrix} \mathbf{w}_{\beta,i}(t) \\ \mathbf{w}_{\dot{\beta},i}(t) \end{bmatrix}, \; i = 1, 2 \text{ and } 3 \\ \mathbf{y}(t) &= \begin{bmatrix} \mathbf{I}_{3\times3} & \mathbf{0}_{3\times3} \end{bmatrix} \begin{bmatrix} \boldsymbol{\beta}_i(t) \\ \dot{\boldsymbol{\beta}}_i(t) \end{bmatrix} + \mathbf{v}_i(t) \end{aligned} \tag{2b}$$

where $\mathbf{x}(t)$, $\mathbf{u}(t)$ and $\mathbf{y}(t)$ are the state vector, input vector and measurement vector by the blade pitch angle, respectively; and $\mathbf{A}$, $\mathbf{B}$ and $\mathbf{C}$ are system matrices representing the state transition, input and measurement matrices, respectively. Uncertain disturbances are given, including the process noise vector $\mathbf{w}(t)$ and measurement noise vector $\mathbf{v}(t)$. This blade pitch system is observable, controllable and stable according to the observability matrix, controllability matrix, pole and Nyquist diagram from Chen [25].

2.5. Fault description

According to the wind turbine reliability analyses [16], the most common faults occur in the blade pitch system. A fault occurring in the blade pitch system can influence the closed-loop control system and the dynamics of a wind turbine. The incorrect pitch of a blade resulting from faults causes asymmetrical forces on the blades and lead to unbalanced rotation in the rotor. Therefore, a fault occurring in the sensors and actuators can affect the system characteristics or lead to inoperable conditions that have resulted in hydraulic leakage, valve blockage or pump blockage [24]. There is a high possibility that a blade pitch system under multiple fault conditions in blades cannot perform a role of an aerodynamic brake properly while large wind loads are acting on the rotor.

Faults of the blade pitch system are mainly categorized by the pitch sensor and actuator fault. To model the faults, the pitch actuator and sensor equations are updated. In this paper, three types of faults in the pitch sensor and actuator of the blade system can be considered: bias value (PSB), fixed output (PSF) in the pitch sensor and stuck actuator (PAS) as shown in Cho et al. [26]. PSB can be represented by a constant offset value that is added to the measurement from the sensor. PSF of the sensor retains the last measurement after fault occurrence. PAS is mainly caused by valve blockage which is mainly due to debris that could clog the valve in the flow in the hydraulic pitch actuator and represents one of the hazards announced by the fault analysis with a level of occurrence and severity by Esbensen and Sloth [24].

Faults to the blade pitch sensor and actuator frequently occur and result in the structural loading of the

turbine because of rotor imbalance, and they affect the stability of the floating platform. Other faults, such as hydraulic leakage and high air content in oil, can occur only by changing the natural frequency and damping ratio in the actuator. Therefore, these uncritical topics are not evaluated in this paper.

3. Fault detection, fault isolation and fault-tolerant control methods

Figure 2 shows the control procedure for a pitch-regulated wind turbine. The baseline controller regulates the wind turbine power production through blade pitch and generator torque control under normal operational conditions. The condition monitoring system with sensors measures the blade pitch angle, tower acceleration, and rotor speed. By using a fault detection and isolation algorithm, the system can detect, isolate, and accommodate faults at an early stage. Upon fault detection, the fault-tolerant controller selects a remedial action based on the protection strategy. If the fault is tolerable, then it can be accommodated by a signal correction in the case of sensor faults. If the situation is intolerable and the wind turbine is not in a safe state, then the controller brings the turbine to a shutdown mode.

3.1 Fault detection

In fault detection, faults in a system and their detection time are determined. Model-based approaches detect faults by comparing the generated residual from the measured pitch angle and threshold. The basic methods for establishing and evaluating the residual are described in this section. Currently, observer methods are the main model-based approaches for detecting faults. In this paper, a Kalman filter, which is a classical method used in fault detection and other fields, is used. Figure 3 shows the basic structure of model-based fault detection. Based on the input command $u(k)$ and measured output $y(k)$, the states and measurements are estimated by an observer. By comparing the measured and estimated values, changes of a state are identified by a threshold.

3.1.1 Observer design based on the discrete-time space model

The discrete system is more suitable for numerical computing and employing an observer than the continuous system. The discrete-time state-space model of the blade pitch system with disturbance and faults in the pitch actuator and sensor can be transferred from the proposed system (2) where the Euler discretization approach is applied.

$$\begin{aligned} \mathbf{x}(k+1) &= \mathbf{\Phi}\mathbf{x}(k) + \mathbf{\Psi}\mathbf{u}(k) + \mathbf{\Gamma}_f \mathbf{f}_A(k) + \mathbf{\Gamma}_d \mathbf{w}(k) \\ \mathbf{y}(k) &= \mathbf{H}\mathbf{x}(k) + \mathbf{\Xi}_f \mathbf{f}_S(k) + \mathbf{\Xi}_d \mathbf{v}(k) \end{aligned} \tag{3}$$

where $\mathbf{\Phi} = \mathbf{I} + \mathbf{A}T$, $\mathbf{\Psi} = \mathbf{B}T$ and $\mathbf{H} = \mathbf{C}$. Here, $\mathbf{\Phi}$, $\mathbf{\Psi}$, $\mathbf{H}$, $\mathbf{\Gamma}_d$, $\mathbf{\Gamma}_f$, $\mathbf{\Xi}_d$, and $\mathbf{\Xi}_f$ are known constant matrices in a discretized system. In addition, T is sampling time and $\mathbf{f}_A(k)$ and $\mathbf{f}_S(k)$ are the actuator and sensor fault vectors described in Cho et al. [26], respectively.

The observer with a healthy case based on the Kalman filter method is designed as follows:

$$\begin{aligned} \hat{\mathbf{x}}(k+1) &= \mathbf{\Phi}\hat{\mathbf{x}}(k) + \mathbf{\Psi}\mathbf{u}(k) + \mathbf{K}(\mathbf{y}(k) - \mathbf{H}\hat{\mathbf{x}}(k)) \\ \hat{\mathbf{y}}(k) &= \mathbf{H}\hat{\mathbf{x}}(k) \end{aligned} \tag{4}$$

where $\hat{\mathbf{x}}(k)$, $\hat{\mathbf{y}}(k)$ and $\mathbf{K}$ are the estimated state vector, estimated output vector, and Kalman gain matrix, respectively.

3.1.2 Residual generation and evaluation

A residual $r(k)$ is the difference between the measured and estimated values described as follows:

$$r(k) = y(k) - \hat{y}(k) \tag{5}$$

A residual energy $J(k)$ is defined by the L_2 norm [27], which is described by the root-mean-square (RMS) of the residual as follows:

$$J(k) = \left\| r(k) \right\|_{2,k} = \left(\sum_{i=1}^{n} r_i^T(k) r_i(k) \right)^{1/2} \tag{6}$$

Because the residual energy in fault cases includes fault information, the generated residual energy should be evaluated by fault detection logic. The residual determines the fault status by applying fault detection logic with threshold J_{th}.

$$\begin{aligned} &J(k) < J_{th}, \ \text{fault} - \text{free} \\ &J(k) > J_{th}, \ \text{fault} \end{aligned} \tag{7}$$

The threshold is generated with bounded uncertainty. Hence, when the residual energy is less than this threshold, the fault-free state is indicated. Otherwise, the fault can be detected. The threshold design procedure using H_∞ optimization and linear matrix inequality (LMI) was described in Cho et al. [26] with more details for the derivation.

If the system is a fault-free state, the residual energy is expressed as

$$J(k) = \left\| r_d(k) \right\|_2 \le \left\| \mathbf{G}_{rd}(z) \right\|_\infty \left\| v \right\|_2 \le \gamma_{\min} \delta_d \tag{8}$$

where $r_d(k)$ is a disturbance residual, $\mathbf{G}_{rd}(z)$ is a disturbance transfer function, $\gamma_{\min}$ is a minimum design parameter for a performance bound and δ_d is a measurement noise boundary. $\mathbf{G}_{rd}(z)$ is defined in frequency domain and $\gamma_{\min}$ is calculated according to LMI in a discrete-time system described in Cho et al. [26]. In addition, δ_d is defined by sensor resolution.

Therefore, the threshold is set as follows:

$$J_{th} = \gamma_{\min} \delta_d \,. \tag{9}$$

3.2 Fault isolation

After a successful fault detection, the main challenge is fault isolation. Fault isolation means determining the type, location, and magnitude of a fault following detection. The fault isolation decision can be made after the residual generator has generated a detection alarm that indicates the occurrence of a fault as presented in Figure 3. This paper suggests a fault isolation algorithm based on a Kalman filter using inference methods [4][28].

Most wind turbines have a single pitch sensor in each blade. As shown in Figure 4 (a), PSF faults cannot be easily distinguished from PAS faults solely by measurements of the pitch angle. However, the nacelle yaw motions are completely different between the two faults illustrated in Figure 4 (b). The reason why nacelle yaw motions are different under PSF and PAS faults depends on whether the pitch actuators are still working or not. The blade is seized in the PAS case and cannot respond to the pitch command (control value). However, the blade can still pitch in the PSF case, but the pitch sensor gives a fixed value and the pitch command is affected by faults, which results in an oscillating irregular pitch angle with a large amplitude than PAS. This leads to a larger yaw motion under PSF, as shown in Figure 4. The pitch command from the pitch controller can be influenced by the difference between reference and measurement values that makes a pitch angle oscillate and consequently a wind turbine unstable that results in the unbalanced rotor. Alternatively, fault isolation can be conducted using measurements of nacelle yaw motions.

Figure 5 shows an algorithm for fault isolation using the single blade pitch angle and nacelle yaw angle measurements. Initially, the trend of the pitch measurement $\beta_{i,k}$ must be determined. If the faulty sensor keeps outputting $\beta_{i,k+1} - \beta_{i,k} = 0$, then the algorithm decides that the fault is PSF or PAS. Then, by comparing the standard deviation of the nacelle yaw angle in normal $\sigma_{Yaw,n}$ and fault conditions $\sigma_{Yaw,f}$, the two faults can be differentiated. Once $\sigma_{Yaw,f}$ is greater than $\sigma_{Yaw,n}$, then the algorithm makes a decision of PSF in the pitch system. Otherwise, the algorithm indicates that there is PAS in the pitch system. To identify PSB, the estimation error should be determined, which can be performed by the residual of the pitch angle from the residual generator. If the fault estimation errors are bounded in a certain range δ, then the algorithm makes a decision that the fault is a PSB.

In the verification procedure, 300 simulations of each fault case were conducted with a duration of 300 s to evaluate the algorithm of fault isolation. The location, magnitude and time of the faults were randomly generated. Once a fault alarm occurred, this algorithm isolated 99% of these faults after 11.5 s. Then, the algorithm makes a fault isolation decision regarding the faults generated from Figure 6. PSF and PAS can be distinguished by the standard deviation values of the nacelle yaw angle σ_{Yaw}.

3.3 Fault-tolerant control

If the sensors and actuators experience faults or are no longer available, then the controller cannot provide the correct control actions for the system. To minimize the potential risks of unexpected faults, new control techniques are needed to manage the faulty system before maintenance is conducted. In this paper, a fault-tolerant control (FTC) scheme is suggested that includes a reconfiguration block and a nominal PI controller after successful fault isolation. The main concept underlying this FTC scheme is to reconstruct the system output y_c to replace the faulty measurement y_f. Because faulty measurement y_f cannot be used with the existing controller, a configuration block must be found that generates a suitable signal y_c from y_f and u_f. Figure 7 shows the block diagram of the control reconfiguration scheme for sensor and actuator faults.

In the scheme, virtual sensors [11] are used to represent the main part of the reconfiguration block for the FTC to conduct signal corrections. The virtual sensor can be used to calculate state vectors by replacing the measurements from the faulty system. The virtual sensor is defined by the state-space model as follows:

$$\begin{aligned} \hat{\mathbf{x}}_{\mathrm{V}}(k+1) &= \mathbf{\Phi}\hat{\mathbf{x}}_{\mathrm{V}}(k) + \mathbf{\Psi}\mathbf{u}_c(k) + \mathbf{K}_{\mathrm{V}}(\mathbf{y}_f(k) - \mathbf{H}_f\hat{\mathbf{x}}(k)) \\ \mathbf{y}_c(k) &= \mathbf{H}_{\mathrm{V}}\hat{\mathbf{x}}_{\mathrm{V}}(k) + \mathbf{P}\mathbf{y}_f(k) \\ \mathbf{u}_f(k) &= \mathbf{u}_c(k) \end{aligned} \tag{10}$$

where $\mathbf{P}$ is a design parameter, and for $\mathbf{P} = \mathbf{0}$, only observed values are used; and $(_{\mathrm{v}})$ represents values in the virtual sensors. The matrix of $\mathbf{H}_{\mathrm{v}}$ is set as equal to measurement matrix $\mathbf{H}$ in Eq. (3). If the fault detection scheme detects any faults in the pitch sensor of the i^{th} blade, the value in $\mathbf{H}_{\mathrm{v}}$ allocated by the faulted sensor has been replaced by 0 in $\mathbf{H}_f$ which means that this sensor is no longer available anymore.

Figure 8 shows the reconfiguration with the virtual sensor after faults. The sensor faults are reflected by the matrix $\mathbf{H}_f$. The virtual sensor estimates the state of the faulty system $\hat{\mathbf{x}}_f$ and replaces the faulty system output. This system output $\mathbf{y}_c$ is improved by using the available sensor values and observing only the difference between the nominal and the faulty output. If this virtual sensor works well, then the state of the virtual sensor $\mathbf{x}_{\mathrm{v}}$ is equivalent to the state of the nominal system $\mathbf{x}$. Hence,

the controller recognizes the same system and reacts in the same way as before.

Actuator faults are critical to the safety of wind turbines when leaving the pitch actuator inoperable regardless of the controller command as shown in Esbensen et al. [24]. Then, the blade cannot be pitched effectively at the large aerodynamic torque above the nominal value. Therefore, pitch actuator faults require a rapid shutdown of the wind turbine as a standard from Jonkman et al. [20]. Once PAS faults are isolated, a safe and fast shutdown of the turbine could be reconfigured to continue power production in response to other faults.

4. Load cases

Floating wind turbines are exposed to a variety of loads in their lifetime. Critical environmental conditions, such as waves, wind gusts, turbulence, and sudden wind direction shifts, are another source of transient loading. For floating wind turbines, appropriate wave conditions must be combined with the wind conditions.

The floating wind turbine operates under variable wind conditions, such as a stochastic wind model that present realistic wind and wave loads. The wind model is based on the IEC 61400-3 design code [31]. A turbulent wind field $U_w(x, y, z, t)$ is commonly modelled by a mean wind and a fluctuating component as described by

$$U_w(t) = U_m + U_f(t) \tag{11}$$

where U_m is the mean wind speed represented as the normal wind profile model (NWP) and U_f is the fluctuating wind for the normal turbulence model (NTM). The turbulent wind U_w is modeled using Turbsim [29] to generate realistic turbulent wind fields according to the Kaimal turbulence model including the turbulence intensity with IEC Class C. The turbulence intensity is a function of the wind speed at the hub height [30][31]. The wave condition is modeled by the JONSWAP wave spectrum. The significant wave height (H_s) and peak period (T_p) are set based on their correlation with wind speed for the Statfjord site in the northern North Sea.

The load cases used to study the dynamic response of the floating wind turbine are given in Table 3. Four independent simulations for turbulent wind and irregular waves were conducted by representing the mean value and standard deviation of the dynamic response for one-hour ensembles.

5. Simulation results and discussion

In this section, a series of simulation results are presented to investigate the performance of the proposed FDI and FTC schemes. Simulations of the wind turbine subjected to a stochastic wind speed are conducted under three different fault conditions: PSB, PSF, and PAS on a single blade and multiple blades.

5.1 Fault detection, fault isolation, and fault-tolerant control with a single fault

5.1.1 Fault detection and isolation results

Faults in the blade pitch system influence the structural dynamics of the wind turbine. Faults in actuators and sensors can be detected effectively by the residual energy and the threshold. When the residual energy exceeds the threshold, a fault alarm is set to 1, which means that a fault is detected. The residual energy should be normalized to adjust the scale factor from the data. The normalized

residual energy J_N is described as follows:

$$J_N(k) = J(k)/J_{th} \tag{12}$$

Figure 9 shows simulation results in connection with the blade pitch angle, normalized residual energy, a fault detection alarm and fault isolation under LC4. In Figure 9 (a), a PSB occurs abruptly after 250 s in the wind turbine corresponding to a sensor bias of -3° on blade 3. Concurrently, an offset value (-3°) occurs between the reference and measurement corresponding to pitch bias. The normalized residual exceeds the threshold, and then the observer detects the blade pitch bias fault immediately by setting to the fault alarm in Figure 9 (b). As shown in Figure 9 (c), the PSB fault can be isolated by the fault isolation algorithm after successful detection.

In the case of PSF and PAS, the pitch angle measurement shows a constant value that is the same as the last measurement value before the faults. The difference between the reference and measurement values makes the pitch angle oscillate irregularly at a large amplitude and the pitch angle difference between fault-free (blades 1, 2) and faulty blade (blade 3) occur as unbalanced rotation. The PSF and PAS simulation results show the same pattern in Figures 10 and 11, respectively, which indicate that faults on blade 3 can be detected based on the fault detection and isolation algorithm.

Cho et al. [26] studied a series of simulations for the reliability of this fault detection algorithm that can detect sensor and actuator faults within a reasonable time after a fault is generated. Therefore, this method can guarantee fault detection at an early stage in the blade pitch system.

5.1.2 Structural response of the floating wind turbine under fault conditions

In this section, numerical results for the fault effects in pitch sensors and actuators are presented. The main objective of the FDI and FTC systems is to avoid unexpected mechanical loads and maximize energy capture. The simulations are conducted to evaluate the proposed FDI and FTC schemes against different fault scenarios. Each simulation has a 1-h duration to reduce the stochastic uncertainty for each load case.

Ocean environmental loads, such as wave and wind loads, excite the structural dynamics of the floating wind turbine. The responses are normalized to adjust the scale factor according to the corresponding values from the fault-free case as described

$$RV_{norm} = \frac{RV_i}{RV_{f-free}} \; i = 1, 2, 3, 4, 5, 6 \tag{13}$$

where RV_{norm} is the response value normalized by the means and standard deviations of the fault-free case $RV_{f\text{-}free}$, and RV_i is the i^{th} response value (1: NC under PSB, 2: FTC under PSB, 3: NC under PSF, 4: FTC under PSF, 5: NC under PAS, and 6: shutdown under PAS).

In particular, the mean and standard deviation (STD) values are calculated for the structural dynamics. Figure 12 shows the effects of a series of fault cases on the normalized mean and STD of the surge, roll, pitch, and yaw motions of a floating wind turbine. The results show that faults affect a significant amount of platform yaw motions compared with the surge, roll and pitch motions because the incident variations in an aerodynamic thrust caused by an unbalanced rotor speed directly affect the instability of platform motion, especially the yaw motion as described by Cho et al. [26].

In the case of PAS, the actuator fault cannot tolerate the reconfiguration block. In cases of platform yaw motion of the FTC in a pitch actuator fault, the fault accommodation is a shutdown to stop wind turbine operations. In this procedure, the standard deviation should be reduced significantly. However, the mean value has been changed because of the unbalanced pitch arrangement even if a wind turbine has undergone shutdown states. As shown in Figure 13, the yaw motion with shutdown presents a positive stable condition. However, the rotor has undergone an unbalanced state because the faulted blade has been seized and the other blades are feathered. Although the results of the nominal and fault-tolerant controllers are similar, changing the dimensionless value generates more considerable differences as described in Table 4. The motions and structural loads of wind turbines can decay to zero by the emergency shutdown. Jiang et al. [18] showed that the dynamic response of wind turbines from the beginning of the shutdown can be unstable but ultimately decay over time.

The PSF fault has a greater effect on dynamic behavior than the PSB and PAS faults. In fault accommodation, the mean and STD results demonstrate that the proposed FTC schemes with signal correction for sensor faults have good performance. The platform motions with FTC schemes in PSB and PSF faults have nearly equivalent values as the fault-free case, which are close to 1. The signal correction brings the floating wind turbine back to normal operational conditions, which means that the FTC scheme with FDI is apparently able to accommodate the fault effects on the pitch system.

Figure 14 shows the platform roll and yaw motions in sensor fault cases for LC4 to check the effectiveness of the FTC for sensor faults. After 250 s, the FDI and FTC algorithms can detect and isolate the faults precisely and conduct signal correction as fault accommodation for faulty sensors, which means that the fault accommodation successfully eliminates unbalanced rotation in the rotor during the PSB and PSF faults. However, unbalanced rotation still occurs in the rotor when a nominal PI controller is used during the faults and leads to instability in the floating wind turbine.

Additionally, the effect of faults on the tower during fault accommodation with the proposed FTC schemes should be presented. Figure 15 shows a comparison of the normalized mean and STD for the tower torsional, fore-aft, and side-to-side bending moments. The bending moments are calculated by the local coordinate system for each component. The results show that the torsional moment is more affected by faults than the fore-aft and side-to-side bending moments. The torsional moment under fault conditions is significant because of the unbalanced aerodynamic loads on the rotor. The PSF fault has a much greater effect on the vibration (STD) than the two other fault cases because of the large oscillation. In fault accommodation, the mean and STD results of the FTC schemes using signal correction from the redundancy sensor demonstrates better performance than the nominal PI controller as shown in Figure 15. The bending moments present nearly equivalent values for both the fault-free case and FTC schemes. In the case of PAS, the bending moments decay to zero with the shutdown.

Figure 16 illustrates the torsional moment and side-to-side bending moment on the tower base in sensor fault cases for LC4 to validate the pitch FTC scheme from 230 to 330 s. After 250 s the FDI and FTC algorithms can detect and isolate the fault precisely and conduct successful signal correction to eliminate the unbalanced rotation during the PSB and PSF faults. The bending moments when a nominal PI controller without the FTC is used increase in the two PSB and PSF cases because of the rotor imbalance and the growth in the aerodynamic thrust force.

5.2 Fault detection, fault isolation, and fault-tolerant control with multiple faults

In this section, the performance of the FDI and FTC schemes is demonstrated for cases with multiple fault scenarios. Simulations for the floating wind turbine subjected to various load cases are conducted considering simultaneous PSB and PSF faults in multiple blades. Faults in actuators and sensors can be detected effectively by the residual energy and the threshold.

Figure 17 shows simulation results in connection with the normalized residual energy, fault alarm, and fault isolation. A PSB corresponding to a sensor bias of -3° abruptly occurs on blade 3 after 100 s, and then a PSF occurs on blade 2 after 200 s. Concurrently, the normalized residual is greater than the threshold, and then the observer detects the PSB and PSF faults immediately by setting to fault alarm as shown in Figure 17 (a) and (b), respectively. Based on the fault isolation algorithm described in Section 3.2, the faults are isolated as shown in Figure 17(c). These results indicate that the presented method can guarantee the FDI at an early stage in the blade pitch system.

Figures 18 and 19 show the platform yaw motion and torsional moment in the tower base for LC4 in PSB and PSF faults at 100 s and 200 s, respectively. The FDI algorithm can detect and isolate faults precisely within 11.5 s. After a successful FDI, the FTC controller with virtual sensors conducts signal correction after 111.5 s. The results indicate that yaw motion with the FTC controller converges to fault-free yaw motion when the FDI is complete. In PSB faults without the FTC controller and only a nominal PI controller, the imbalanced loads act on the rotor representing the unstable values of platform yaw.

Moreover, the occurrence of a PSF fault in blade 2 after 200 s decreases of the stability of the wind turbine. More precisely, the FTC scheme with the FDI demonstrates a highly effective fault accommodation. After the FDI, the FTC controller is well activated in 211.5 s and control is gradually restored as evidenced by the convergence of the platform yaw in the FTC (red line) case with the line of the fault-free case. However, without the FTC, two faults are observed in the rotor in blades 2 and 3; therefore, the platform yaw with a nominal PI controller is magnified over time to a greater degree than that observed with fault-free yaw motion. The torsional moment in the tower base in Figure 19 presents similar behavior in Figure 18. Those figures represent the effectiveness of the FTC, which means that the system can return to a normal state.

6. Conclusions

Fault detection and isolation techniques should be applied to floating wind turbines for the detection and isolation of unexpected faults at an early stage to prevent catastrophic failures. Here, a fault detection method is suggested based on a Kalman filter with focus on blade pitch actuator and sensor faults. In fault detection, a Kalman filter is used for residual generation and a threshold is used for detecting fault conditions in the blade pitch actuators and sensors. In fault isolation, a single blade pitch angle and nacelle yaw angle measurement are employed to isolate faults in the blade pitch system by the inference method. Based on fault isolation logic, the fault isolation decision can be made by comparing the measurement values of the blade pitch and nacelle yaw motion.

Two fault-tolerant control schemes are suggested for reconfigurations using a virtual sensor for sensor faults and shutdown for actuator faults. The FTC controller accommodates the PSB and PSF faults by correcting the system output $\mathbf{y}_c$ with the virtual sensor. These FTC schemes can accommodate single and multiple sensor faults. If the FTC controller works well, then the system recognizes the nominal system and reacts in the same way as before. However, faults in the pitch actuator that are intolerable require another wind turbine FTC method. Once the PAS faults are isolated, an emergency shutdown

of the wind turbine should be conducted to prevent other failures.

The results of the numerical simulations clearly indicate the effectiveness of the proposed FDI and FTC schemes for load cases with faults. The proposed FDI method can effectively detect and isolate all three faults (PSB, PSF, and PAS) at an early stage. With the proposed FTC strategy, the system response in simulations with single and multiple faults is close to the response of wind turbines in the fault-free condition, which means that the FTC scheme can identify and correct faults within a reasonable time. Finally, the proposed FDI and FTC schemes can be easily applied in practice.

Acknowledgments

This work was supported by the MIT-NTNU-Statoil Wind Turbine Program (Project No. 40136503) funded by Statoil. The authors gratefully acknowledge the supports of Statoil and the Research Council of Norway through the Centre for Autonomous Marine Operations and Systems (AMOS) at NTNU for the present study.

References

[1] Global Wind statistics 2015, Global Wind Energy Council, 2016.

[2] The European offshore wind industry – key trends and statistics 2015. The European Wind Energy Association, 2016.

[3] Dinwoodie I, McMillan D, Revie M, Lazakis I, Dalgic Y. Development of a combined operational and strategic decision support model for offshore wind. *Energy Procedia* 2013; 35: 157-166.

[4] Chen W, Ding S X, Haghani A, Naik A, Khan A Q and Yin S. Observer-based FDI Schemes for Wind Turbine Benchmark. *Proceedings of the 18th IFAC World Congress* (Milano: Italy) 2011, 7073 – 7078

[5] Wei X, Verhaegen M, Engelen van T. Sensor fault detection and isolation for wind turbines based on subspace identification and Kalman filter techniques. *International Journal of Adaptive Control and Signal Processing* 2010; 24.8: 687-707.

[6] Malik H and Mishra S. Application of Probabilistic Neural Network in Fault Diagnosis of Wind Turbine Using FAST, TurbSim and Simulink. *Procedia Computer Science* 2015; 58: 186-193.

[7] Dong J and Verhaegen M. Data driven fault detection and isolation of a wind turbine benchmark. *IFAC Proceedings Volumes* 2011; 44.1: 7086-7091.

[8] Santos P, Villa L, Reñones A, Bustillo A, and Maudes J. An SVM-based solution for fault detection in wind turbines. *Sensors* 2015; 15.3: 5627-5648.

[9] Ghane M, Nejad AR, Blanke M, Gao Z and Moan T. Statistical fault diagnosis of wind turbine drivetrain applied to a 5MW floating wind turbine. *Journal of Physics: Conference Series* 2016; 753 052017

[10] Feng Z, Liang M. Fault diagnosis of wind turbine planetary gearbox under nonstationary conditions via adaptive optimal kernel time–frequency analysis. *Renewable Energy* 2014; 66:468-77.

[11] Blanke M, Kinnaert M, Lunze J, Staroswiecki M, Schröder J. Diagnosis and fault-tolerant control:

513 2nd edition. Berlin: Springer; 2010.

514 [12] Shi F, Patton R. An active fault tolerant control approach to an offshore wind turbine model.
515 *Renewable Energy* 2015; 75: 788-98.

516 [13] Seron MM, De Doná JA, Richter JH. Integrated sensor and actuator fault-tolerant control.
517 *International Journal of Control* 2013; 86(4): 689-708.

518 [14] Fan L and Song Y. Neuro-adaptive model-reference fault-tolerant control with application to
519 wind turbines. *IET control theory & applications* 2012; 6.4: 475-486.

520 [15] Vidal Y, Tutivén C, Rodellar J and Acho L. Fault diagnosis and fault-tolerant control of wind
521 turbines via a discrete time controller with a disturbance compensator. *Energies* 2015; 8.5: 4300-4316.

522 [16] Carroll J, McDonald A and McMillan D. Failure rate, repair time and unscheduled O&M cost
523 analysis of offshore wind turbines. *Wind Energy* 2016; 19:1107-1119. DOI: 10.1002/we.1887

524 [17] Bachynski EE, Etemaddar M, Kvittem MI, Luan C and Moan T. Dynamic analysis of floating
525 wind turbines during pitch actuator fault, grid loss, and shutdown. *Energy Procedia* 2013; 35: 210-222.

526 [18] Jiang Z, Karimirad, M and Moan T. Dynamic response analysis of wind turbines under blade
527 pitch system fault, grid loss, and shutdown events. *Wind Energy* 2014; 17: 1385-1409. DOI:
528 10.1002/we.1639

529 [19] Etemaddar M, Blanke M, Gao Z and Moan T. Response analysis and comparison of a spar-type
530 floating offshore wind turbine and an onshore wind turbine under blade pitch controller faults. *Wind*
531 *energy* 2016; 19: 35-50. DOI: 10.1002/we.1819

532 [20] Jonkman J, Butterfield S, Musial W and Scott G. Definition of a 5-MW reference wind turbine
533 for offshore system development *Technical Report NREL/TP-500-38060* USA, 2009

534 [21] Jonkman J. Definition of the floating system for Phase IV of OC3 *Technical Report NREL/TP-*
535 *500-47535* USA, 2010

536 [22] Bachinski E. Simo-Riflex-Aerodyn manual. *MARINTEK Technical Report* Norway, 2014

537 [23] Larsen TJ and Hanson TD. A method to avoid negative damped low-frequency tower vibration
538 for a floating, pitch controlled wind turbine. *Journal of Physics: Conference Series* 2007; **75** 012073.

539 [24] Esbensen T and Sloth C. Fault diagnosis and fault-tolerant control of wind turbines. Master's
540 thesis, Aalborg University, Aalborg, Denmark, 2009

541 [25] Chen C-T. Linear system theory and design: 3rd edition. Oxford University press; 1999.

542 [26] Cho S, Gao Z and Moan T. Model-based fault detection of blade pitch system in floating wind
543 turbines. *Journal of Physics: Conference Series* 2016; **753**: 092012.

544 [27] Ding SX. Model-based fault diagnosis technique: design schemes, algorithms and tools: 2nd
545 edition. London: Springer; 2013.

546 [28] Isermann R. Model-based fault-detection and diagnosis – status and applications. *Annual*
547 *Reviews in Control* 2005; **29**: 71-85

548 [29] Jonkman J and Kilcher L. TurbSim User's Guide *Technical Report NREL* USA, 2012

549 [30] IEC 61400-1: Wind turbines – part 1: Design requirements. International Electrotechnical
550 Commission. 2005.

551 [31] IEC 61400-3: Wind turbines – Part 3: Design requirements for offshore wind turbines.
552 International Electrotechnical Commission. 2005.

Table 1. Properties for the NREL 5 MW wind turbine [20]

Rated Power (MW)	5
Rotor orientation, Configuration	Upwind, 3 blades, horizontal axis
Rotor diameter (m)	126
Hub height from the mean water level (m)	90
Cut-in, rated, cut-out wind speed (m/s)	3, 11.4, 25
Cut-in, rated rotor speed (rpm)	6.9, 12.1
Max pitch rate (°/s)	8
Gearbox ratio	97

Table 2. Properties for the OC3-Hywind floater [21]

Water depth (m)	320
Draft (m)	120
Diameter above taper (m)	6.5
Diameter below taper (m)	9.4
Center of mass (m)	(0, 0, -89.9115)
Mass, including ballast (kg)	7.466×10^6
Mass moment of inertia, I_{xx} and I_{yy} (kg·m^2)	4.229×10^9
Mass moment of inertia, I_{zz} (kg·m^2)	1.642×10^8

Table 3. Wind and wave conditions

Load case	U_w (m/s)	Turbulent model	H_s (m)	T_p (s)
1	11.2	IEC Class C	3.2	10.0
2	14		3.62	10.30
3	17		4.2	10.50
4	20		4.8	10.80

Table 4. Mean and dimensionless values of platform yaw under LC4

	Yaw (Mean)	Yaw (Dimensionless)
Fault-free	-0.1458	1
NC in PAS fault	-0.1303	0.8937
Shutdown in PAS fault	-0.8083	5.55439

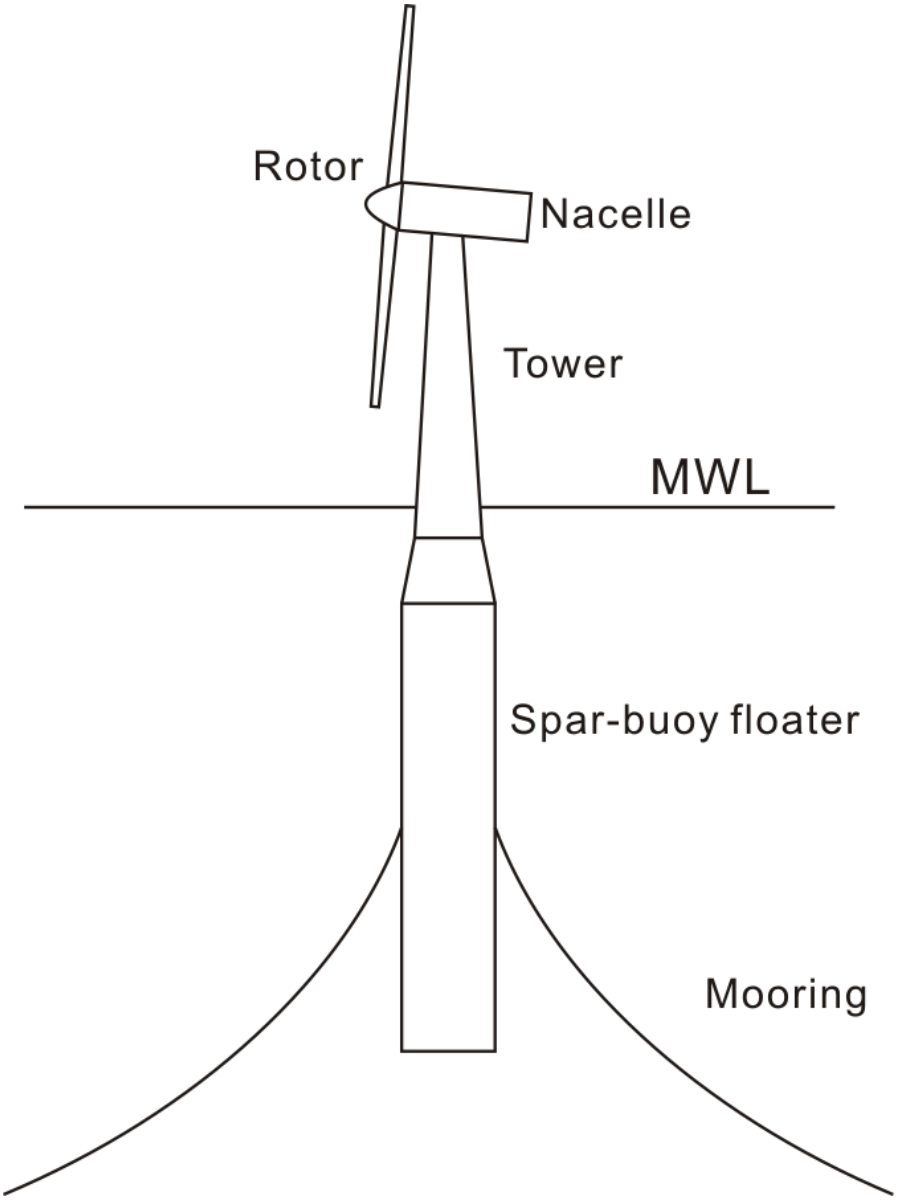

Figure 1. Schematic view of the floating wind turbines.

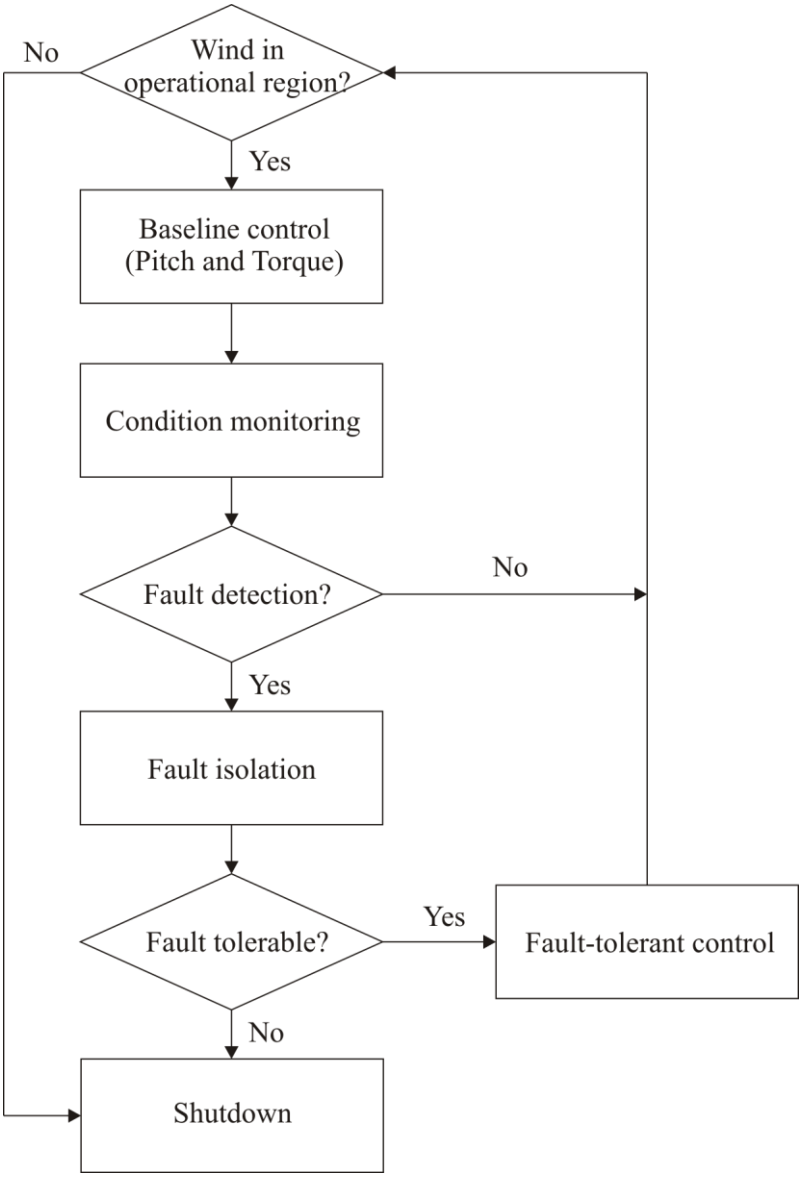

Figure 2. Control procedure for a wind turbine with FDI and FTC.

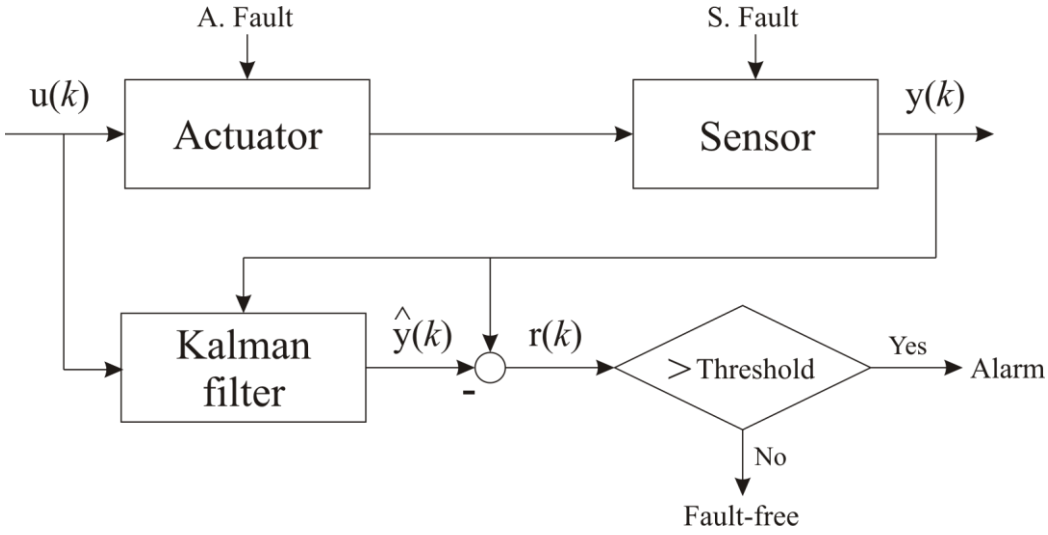

Figure 3. Scheme of observer-based fault detection in the blade pitch system.

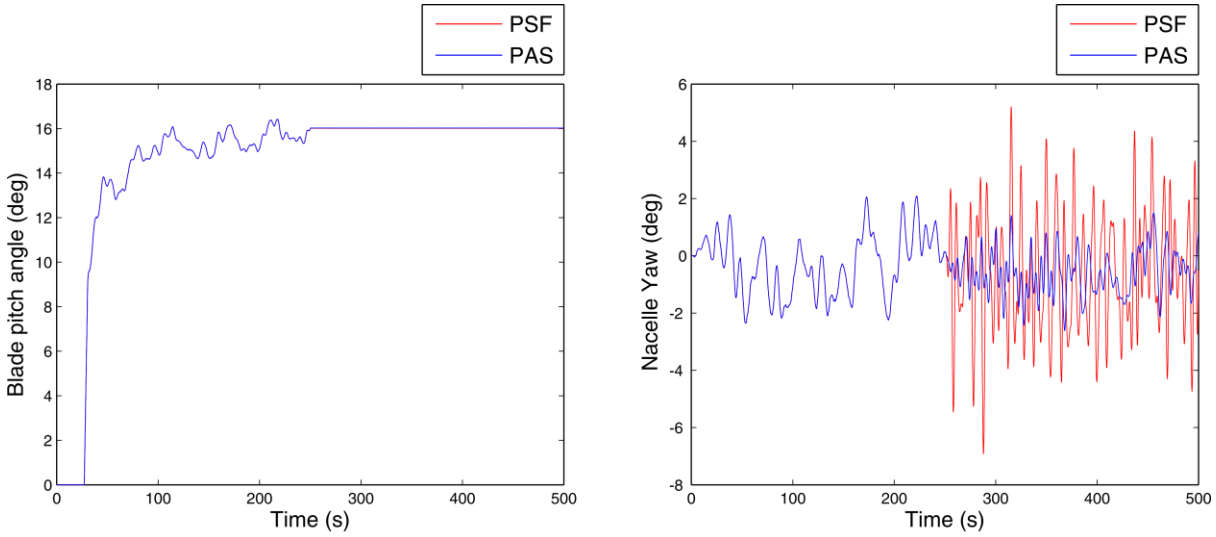

(a) Blade pitch angle (b) Nacelle yaw

Figure 4. Comparison of the effects of PSF and PAS faults on the blade pitch angle and nacelle yaw.

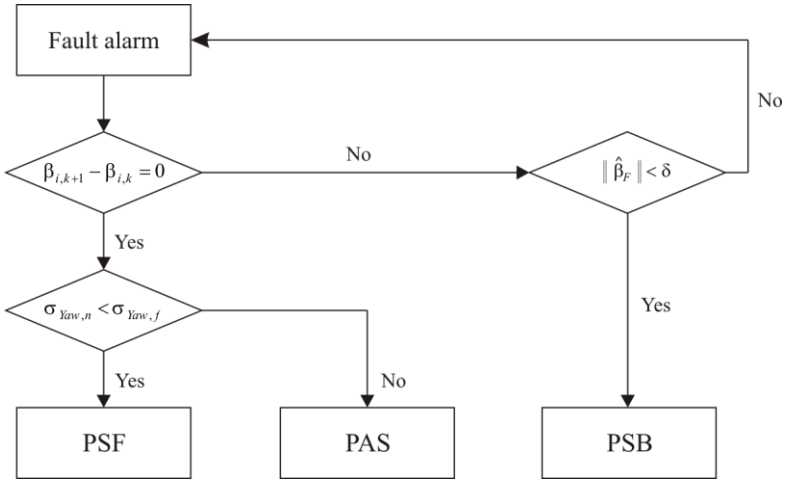

Figure 5. Algorithm of fault isolation with a single pitch sensor

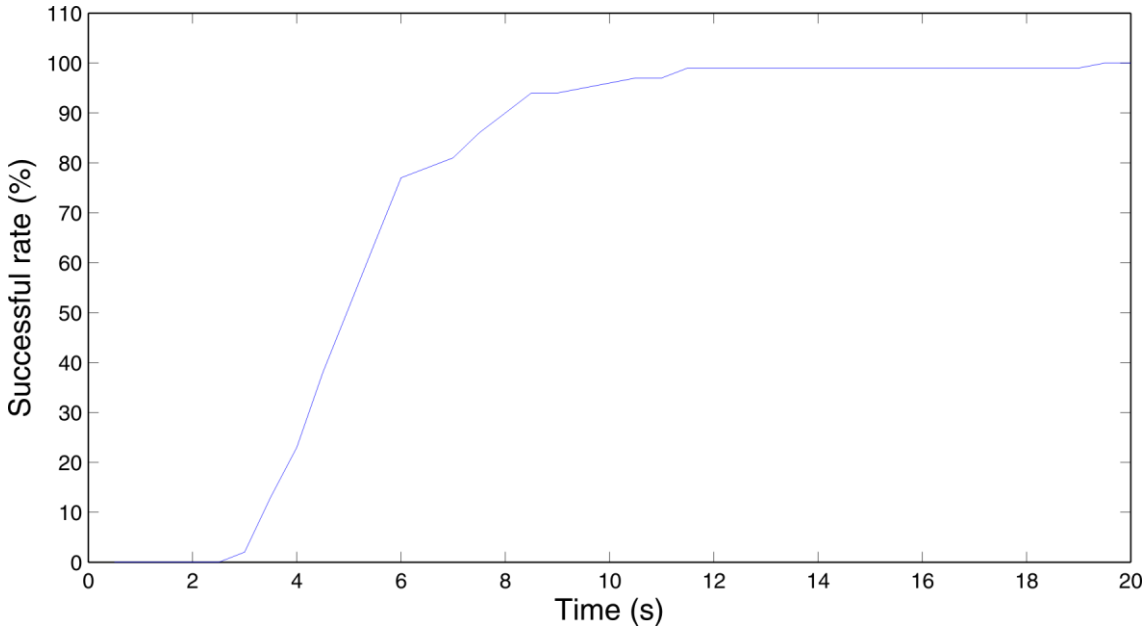

Figure 6. Successful rates of fault isolation at each number of steps.

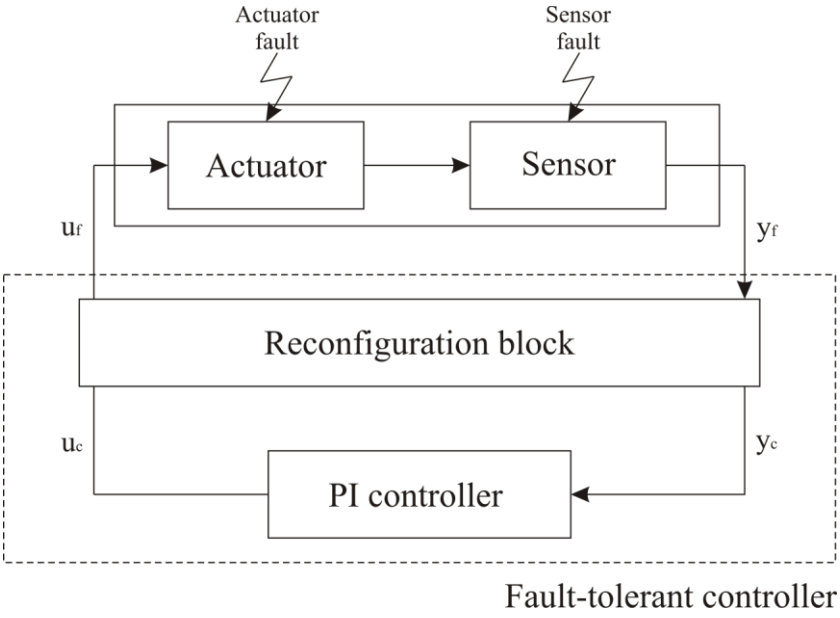

Figure 7. Control reconfiguration for sensor and actuator faults.

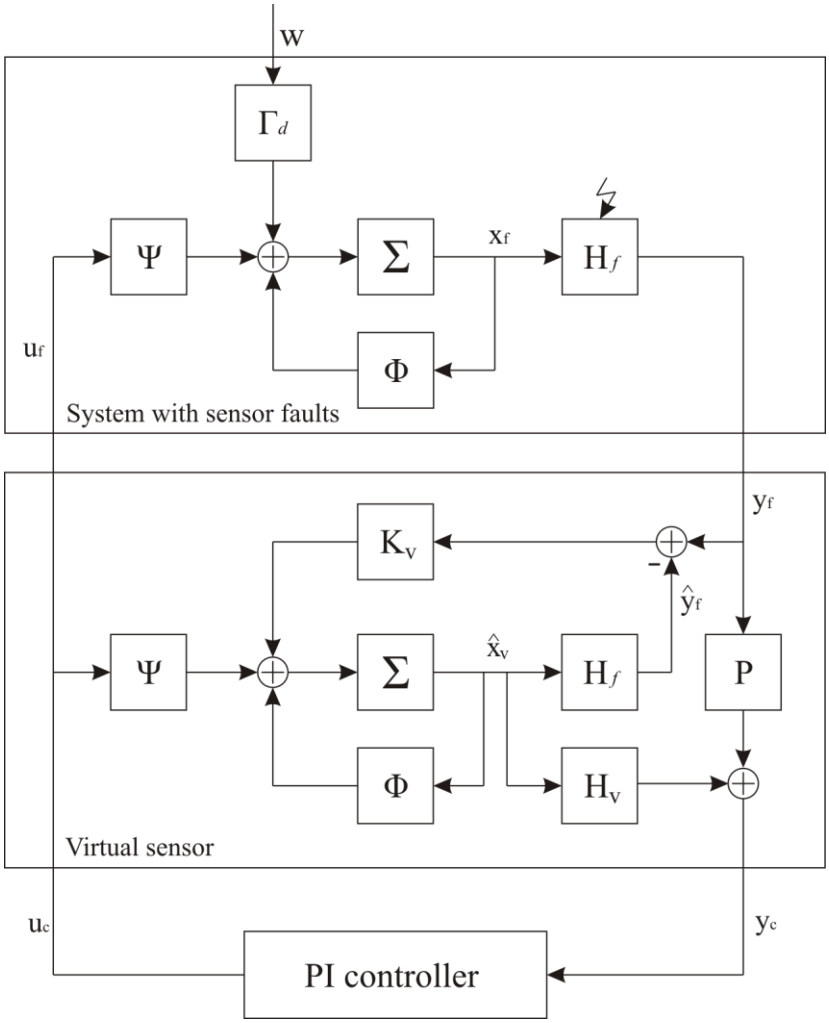

Figure 8. Reconfiguration with a virtual sensor after sensor faults

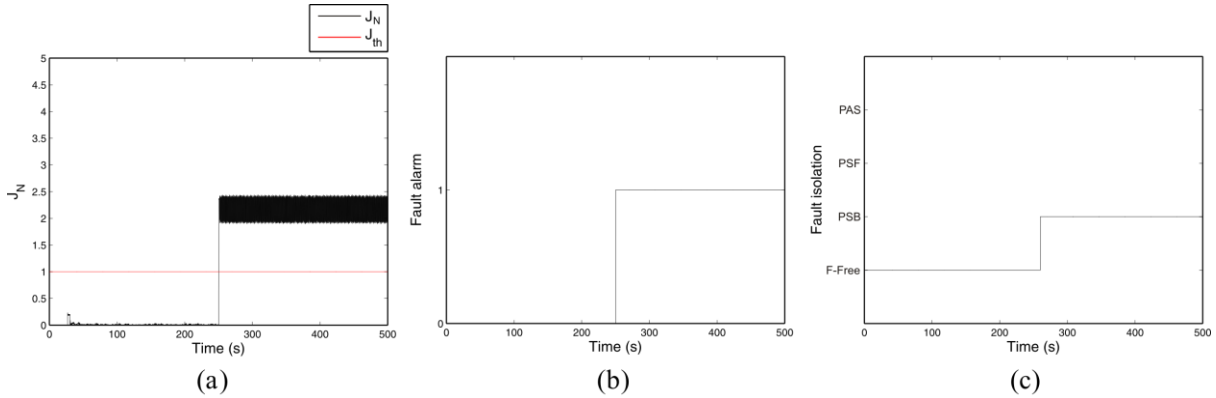

Figure 9. Simulation results of the PSB case corresponding to the blade pitch angle under LC4: (a) normalized residual energy, (b) fault detection alarm, and (c) fault isolation.

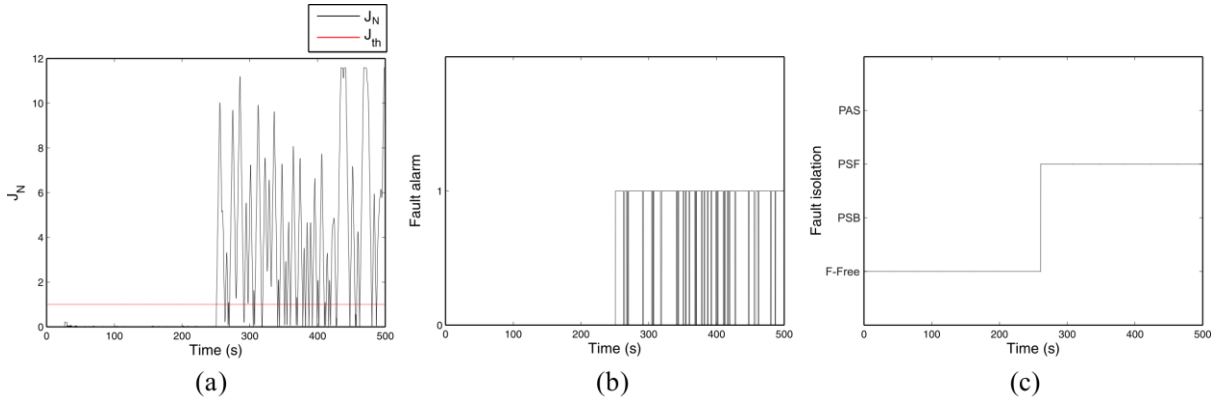

Figure 10. Simulation results of the PSF case corresponding to the blade pitch angle under LC4: (a) normalized residual energy, (b) fault detection alarm, and (c) fault isolation.

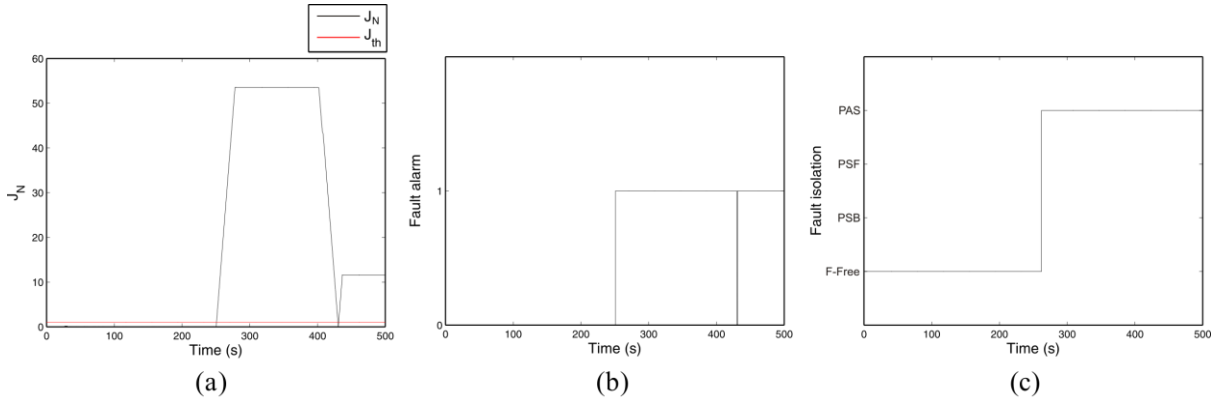

Figure 11. Simulation results of the PAS case corresponding to the blade pitch angle under LC4: (a) normalized residual energy, (b) fault detection alarm, and (c) fault isolation.

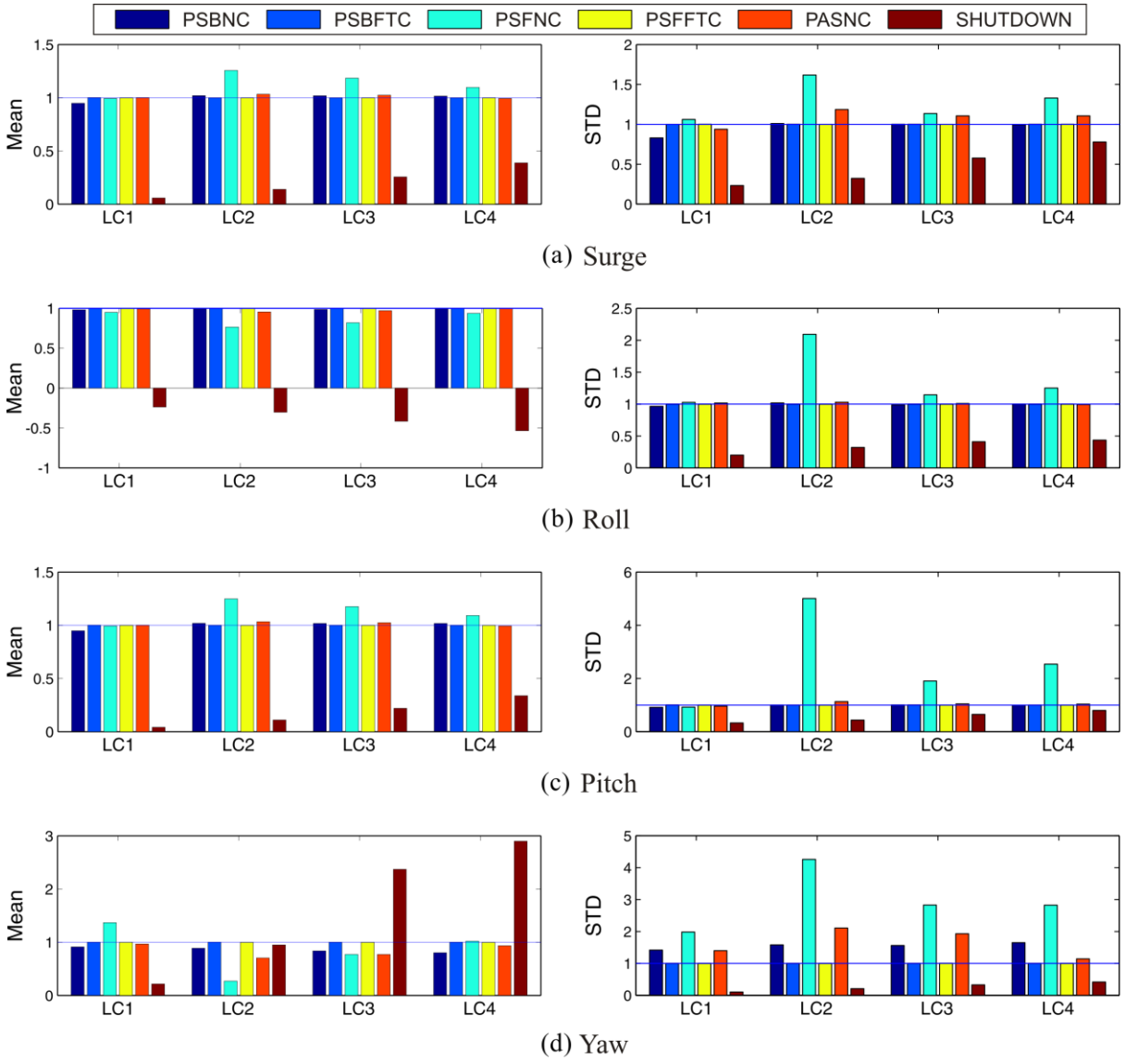

Figure 12. Mean values and standard deviations (STDs) of the platform surge, roll, pitch, and yaw motions for the floating wind turbine under PSB, PSF and PAS fault conditions with nominal PI and fault-tolerant controllers (blue line: fault-free; dark blue bar: nominal PI controller with PSB; blue bar: FTC controller with PSB; cyan bar: nominal PI controller with PSF; yellow bar: FTC controller with PSF; orange bar: nominal PI controller with PAS; and brown bar: shutdown).

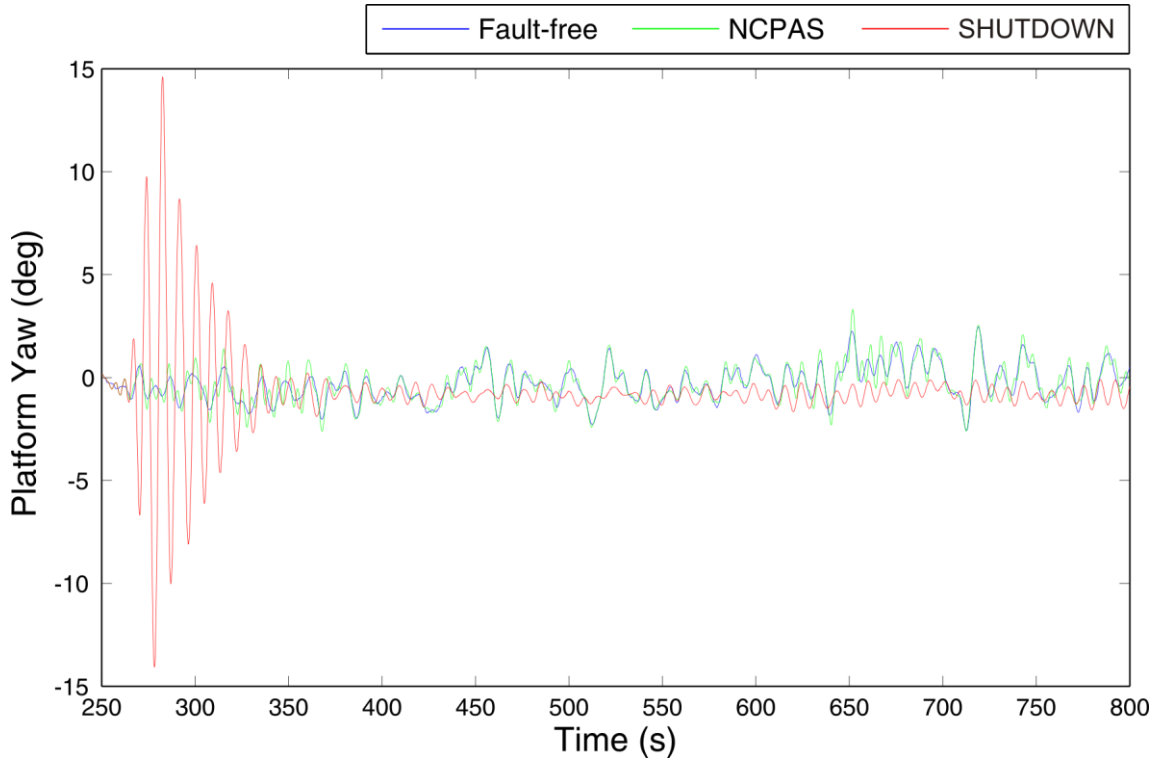

Figure 13. Platform yaw motion after PAS fault (blue line: fault-free; green line: nominal controller with PAS; and red line: shutdown with PAS).

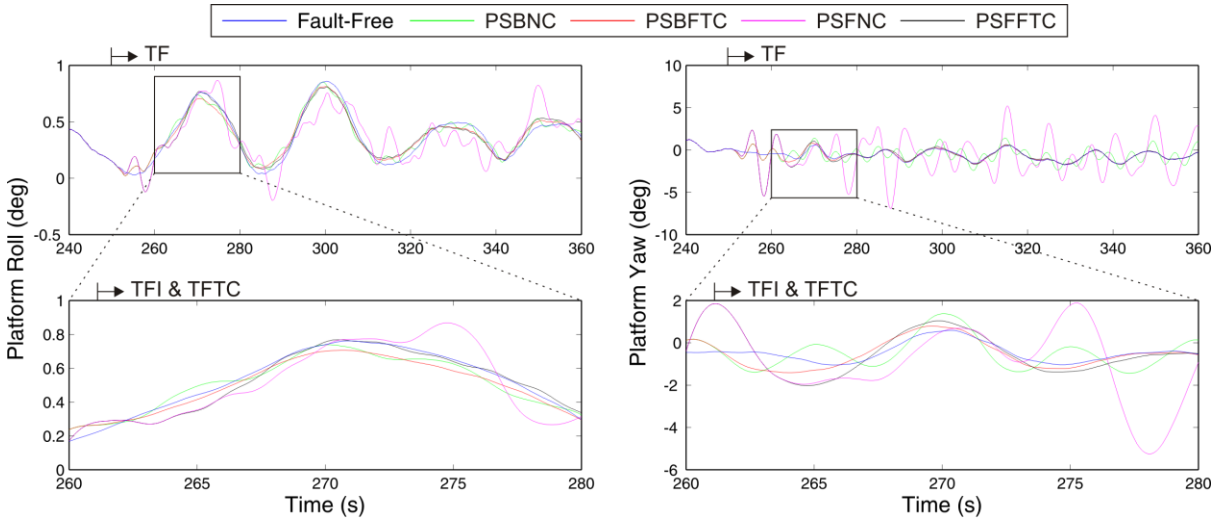

(a) Roll (b) Yaw

Figure 14. Comparison of the platform pitch and yaw motions under PSB and PSF fault conditions with nominal PI and fault-tolerant controllers under LC4.

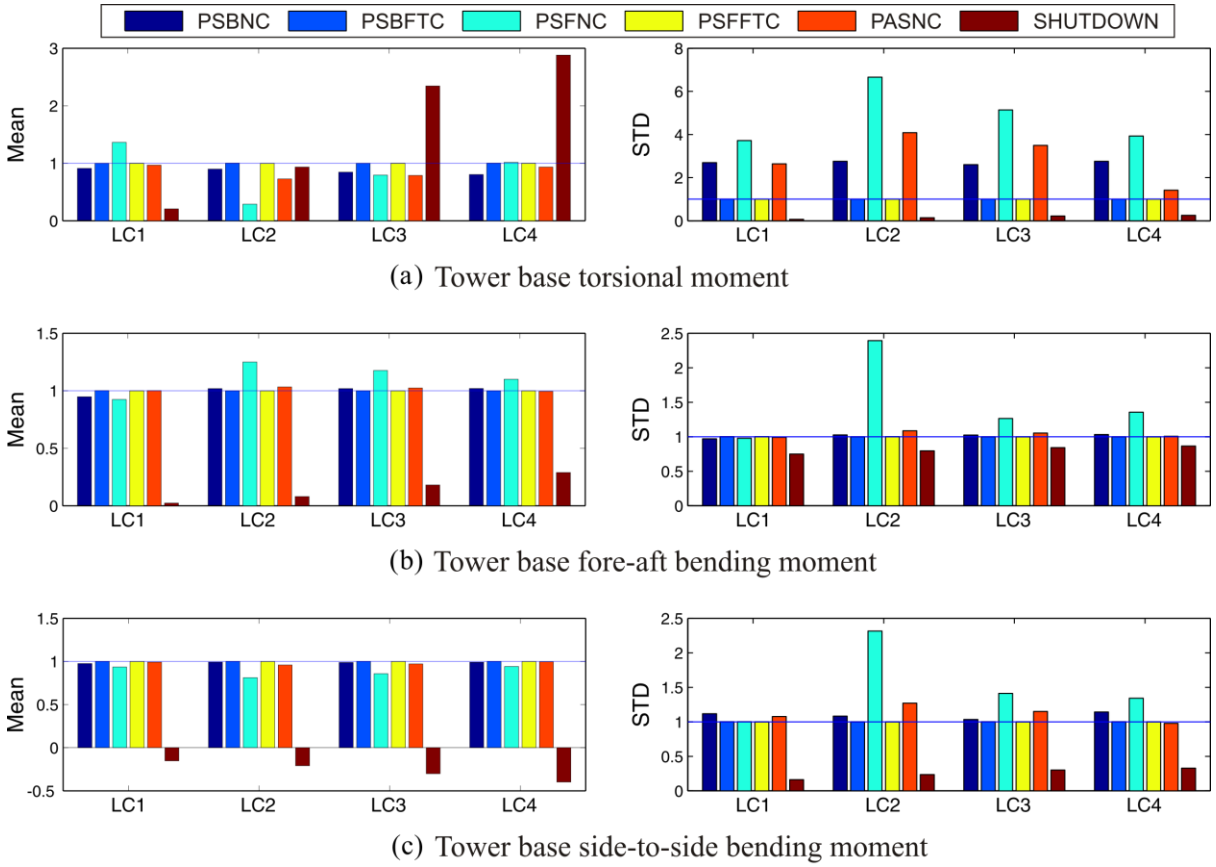

Figure 15. Mean values and standard deviations (STDs) of the torsional, fore-aft and side-to-side bending moments for the floating wind turbine under PSB, PSF and PAS fault conditions with nominal PI and FTC controllers (blue line: fault-free; dark blue bar: nominal PI controller with PSB; blue bar: FTC controller with PSB; cyan bar: nominal PI controller with PSF; yellow bar: FTC controller with PSF; orange bar: nominal PI controller with PAS; and brown bar: shutdown).

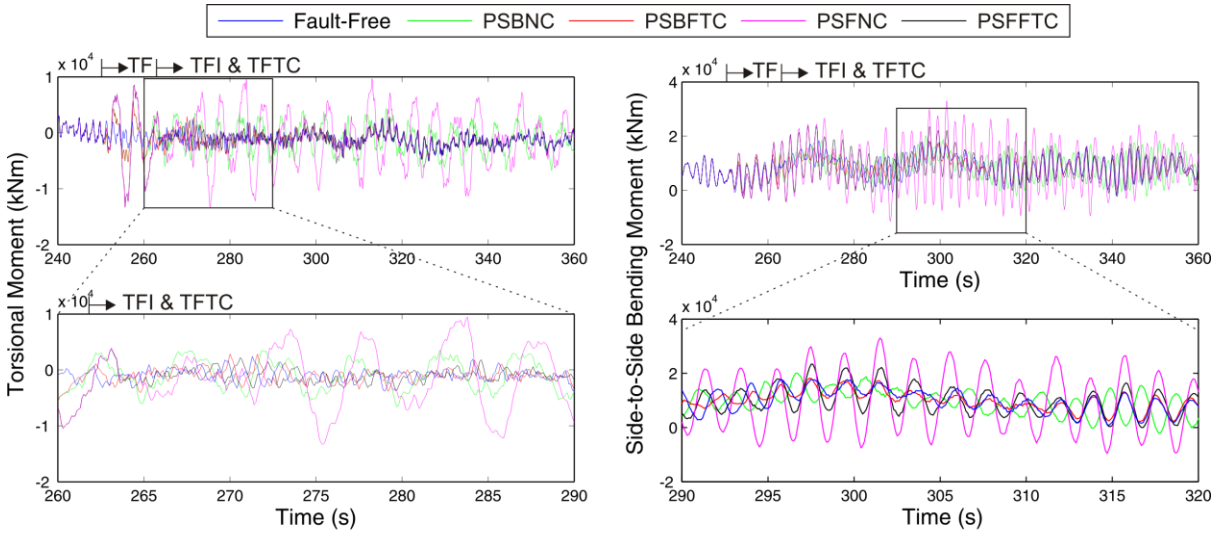

(a) Tower base torsional moment

(b) Tower base side-to-side bending moment

Figure 16. Comparison of the torsional and side-to-side bending moments under PSB and PSF fault conditions with nominal PI and fault-tolerant controllers under LC4.

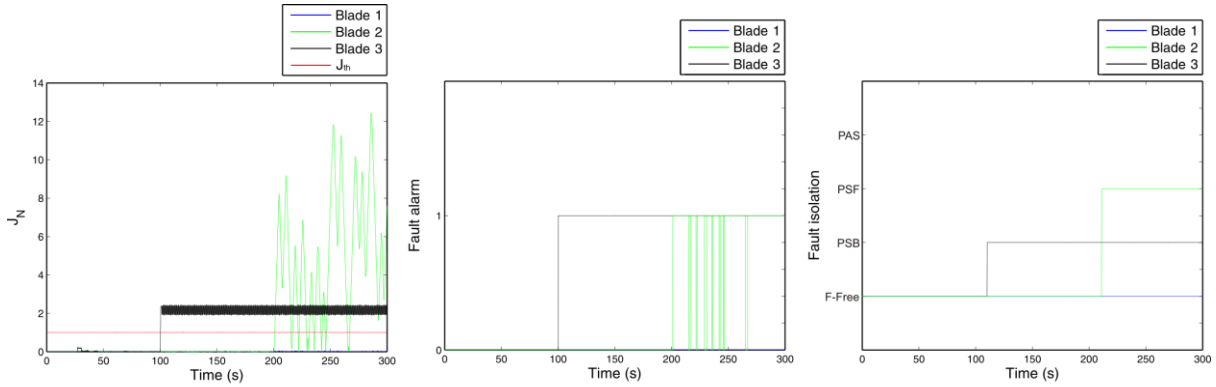

Figure 17. Simulation results of the PSB and PSF cases corresponding to the blade pitch angle: (a) normalized residual energy, (b) fault detection alarm and (c) fault isolation under LC4.

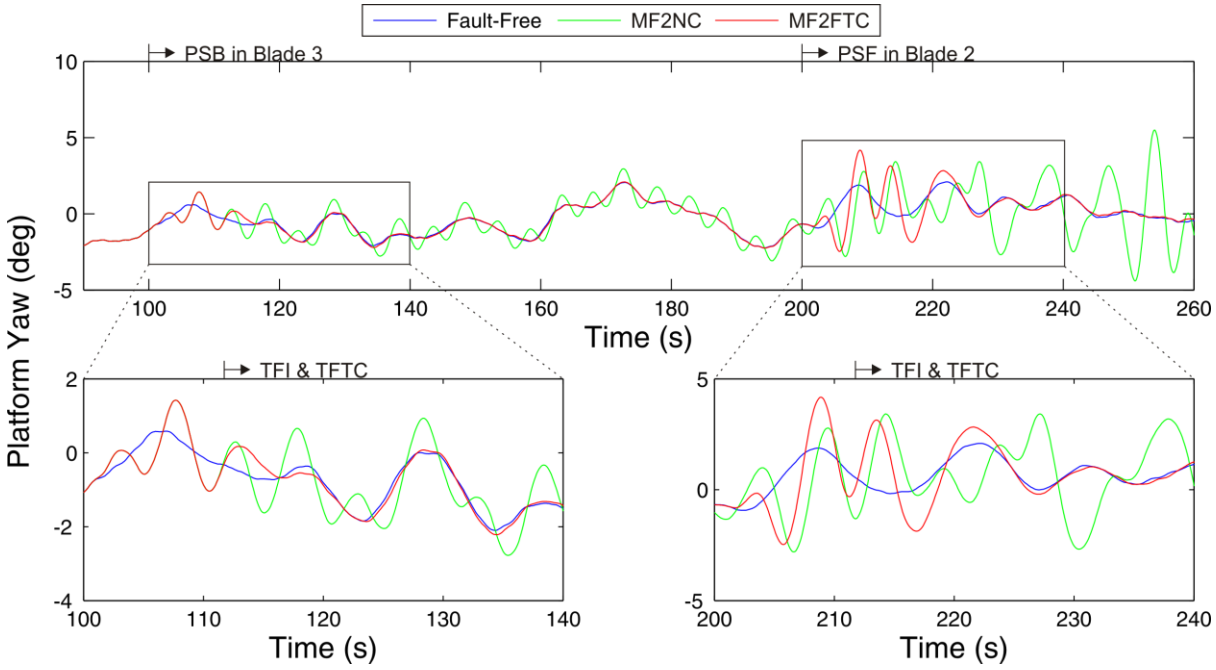

Figure 18. Comparison of the platform yaw motion under PSB and PSF fault conditions with nominal PI and fault-tolerant controllers under LC4.

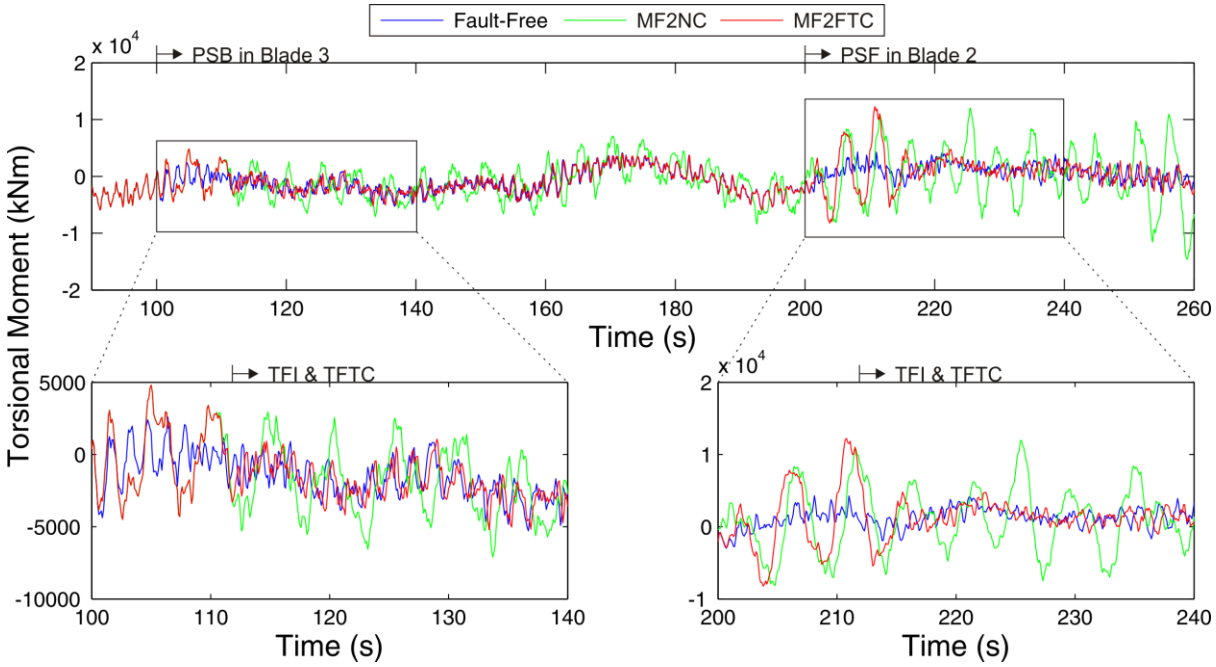

Figure 19. Comparison of the tower base torsional moment under PSB and PSF fault conditions with nominal PI and fault-tolerant controllers under LC4.